Proceedings of the ASME 2016 Dynamic Systems and Control Conference
DSCC2016
October 12-14, 2016, Minneapolis, MN, USA

DSCC2016-9905

NEAR ENERGY OPTIMAL CONTROL ALLOCATION FOR DUAL-INPUT OVER-ACTUATED SYSTEMS

Molong Duan
Department of Mechanical Engineering
University of Michigan, Ann Arbor, MI, USA
molong@umich.edu

Chinedum Okwudire
Department of Mechanical Engineering
University of Michigan, Ann Arbor, MI, USA
okwudire@umich.edu

ABSTRACT

This paper proposes a method for near energy optimal allocation of control effort in dual-input over-actuated systems using a linear time-invariant (LTI) controller. The method assumes a quadratic energy cost functional, and the non-causal energy optimal control ratio within the redundant actuation space is defined. Near energy optimal control allocation is addressed by using a LTI controller to align the control inputs with a causal approximation of the energy optimal control ratio. The use of a LTI controller for control allocation leads to low computation burden compared to techniques in the literature which require optimization at each time step. Moreover, the proposed method achieves broadband, near optimal control allocation, as opposed to traditional allocation methods which make use of a static system model for control allocation. The proposed method is validated through simulations and experiments on an over-actuated hybrid feed drive system. Significant improvements in energy efficiency without sacrificing positioning performance are demonstrated.

1. INTRODUCTION

Over-actuation in motion delivery mechanisms means using more effectors than the mechanism's degree of freedom [1]. Over-actuated systems help to enhance fault tolerance, accuracy, energy efficiency, etc., and are therefore widely adopted in modern motion control applications [1–8]. For example, redundant thrusters employed in aerospace applications enable reconfigurable flight control, which can address thruster failures and improve safety [4]. In servo systems, over-actuation is used to improve motion range [2], precision [7] or energy efficiency [1]. Over-actuation also has the prospect of addressing structural flexibility related issues in lightweight structures envisioned for the next generation of advanced motion systems in the semiconductor industry [3].

The control of over-actuated systems requires an appropriate method to translate the desired motion and total actuation effort to the control space defined for redundant actuation [9]. One common approach is to use control allocation methods in which, generally, a two-stage framework (i.e., a high level motion controller and a dedicated allocator distributing the control efforts) is employed [10]. The high level motion controller (which does not usually consider actuation redundancy) can be designed with traditional control methods (e.g. backstepping [11], model reference control [12], sliding mode control [5], etc.). The core idea of the allocator is to establish an optimization space based on the redundancy in actuation [13,14]. Control allocation problems are categorized into strong and weak input redundancy cases [15]. Mathematically, they are formulated as time domain constrained optimization problems [12]. The computational load and performance gain of representative computational methods (i.e., redistributed pseudoinverse, pseudoinverse based quadratic programming and fixed-point methods) are compared in [12]. It is shown that control allocation can yield same results as optimal control methods while providing additional benefits of constraint handling [16].

One drawback of some available control allocation methods arises from their time-domain optimization nature, which requires the optimization to be implemented for every time step and thus leads to high computational load. Computationally efficient algorithms (e.g., [12]) can be used, however true optimality cannot always be guaranteed [17]. Another limitation arises from the static model assumed by most methods [10–12,15,17]. A static model undermines the allocator's ability to optimally distribute non-static control efforts. Though non-static models [10] and longer optimization horizons [18] can be introduced into the optimization process, they further increase computational load and complicate implementation.

In this paper, based on a causal approximation of the energy optimal control ratio (proposed by the authors in prior work [19,20]), an near energy optimal, linear time-invariant allocator for dual-input over-actuated systems is introduced, as an alternative to time domain optimization methods, thereby greatly reducing the allocator's computational load. Moreover, the proposed allocator uses the complete dynamic model of the over-actuated system, thus enabling broadband control effort distribution among redundant actuators.

The paper is organized as follows. In Section 2, some background on over-actuated systems, the energy optimal control ratio and its causal approximation are provided, followed by the methodology, stability analysis and design guidelines for the proposed near energy optimal control allocator. The proposed allocator is then implemented on an over-actuated hybrid feed drive system in Section 3, where simulation and experimental results are provided for validation. Conclusions and future work are presented in Section 4.

2. BACKGROUND

2.1. OVER-ACTUATED SYSTEMS

Consider a linear time-invariant (LTI) system given by the equation

$$\mathbf{y} = \mathbf{G}\mathbf{u} + \mathbf{G}_\mathrm{d}\mathbf{d} \tag{1}$$

where $\mathbf{y} \in \mathbb{R}^{n_y}$ is the output of the system, while $\mathbf{u} \in \mathbb{R}^{n_u}$, $\mathbf{d} \in \mathbb{R}^{n_d}$ are the control and disturbance inputs into the system, respectively. One minimal realization of this system is

$$\begin{aligned} \dot{\mathbf{x}} &= \mathbf{A}\mathbf{x} + \mathbf{B}_\mathrm{u}\mathbf{u} + \mathbf{B}_\mathrm{d}\mathbf{d} \\ \mathbf{y} &= \mathbf{C}_\mathrm{y}\mathbf{x} + \mathbf{D}_\mathrm{u}\mathbf{u} + \mathbf{D}_\mathrm{d}\mathbf{d} \end{aligned} \tag{2}$$

Following the definition in [15], the LTI system is defined to be strongly input redundant if

$$\mathrm{Ker}\left(\begin{bmatrix}\mathbf{B}_\mathrm{u}\\ \mathbf{D}_\mathrm{u}\end{bmatrix}\right) \neq \varnothing \tag{3}$$

and weakly input redundant system if

$$\mathrm{Ker}\left(\lim_{s\to 0}\mathbf{G}(s)\right) \neq \varnothing \tag{4}$$

where Ker yields the kernel (null space) of the corresponding matrices. Note that strong input redundancy requires the existence of control inputs which are directly cancellable before affecting the state dynamics. This condition is relaxed in the weak input redundancy case to focus on input alignments that would not affect the steady state outputs of the system. From an engineering point of view, it is believed that the definition of weak input redundancy is more practical, as strong input redundancy can only be achieved by either exact collocation of the actuation inputs or severe truncation of high frequency dynamics [13]. Therefore, in this paper, weak input redundancy is assumed, and it is shown that the original steady state definition in Eq. (4) can be expanded to broadband cases.

2.2. ENERGY OPTIMAL CONTROL RATIO AND ITS CAUSAL APPROXIMATION

Due to system redundancy, there exists a family of state and input trajectories that yield a given output trajectory [15]. The concept of energy optimal control ratio [19] is used, within a specific family, to specify the relationship of the control inputs to approach energy optimality. In this paper, the most basic over-actuated system, $\mathbf{G} = [G_1, G_2]$, with two inputs $\mathbf{u} = [u_1, u_2]^\mathrm{T}$, a single output y and a scalar disturbance d is considered. Assume a nominal control input $\mathbf{u}_0$ which yields a desirable output y_0 under disturbance d_0, i.e.,

$$\mathbf{G}\mathbf{u}_0 = y_0 - G_\mathrm{d}d_0 \tag{5}$$

The family of control signals which replicate y_0 under d_0 formulates a set Ω, given by

$$\Omega(\mathbf{u}_0) \triangleq \left\{\mathbf{u} \in \mathbb{R}^2 : \mathbf{G}(\mathbf{u}_0 - \mathbf{u}) = 0\right\} \tag{6}$$

Consider the variation of a member of this set; it should satisfy

$$G_1\delta u_1 + G_2\delta u_2 = 0 \tag{7}$$

to remain in Ω. It is desirable to pick the energy optimal member from the set Ω for control, since every member of the set has the same impact on the system. Set Ω formulates the optimization space in the over-actuated system, and it is nonempty due to the system's redundant nature.

Consider the typical quadratic energy cost functional

$$J \triangleq \int\left(\mathbf{u}^\mathrm{T}\mathbf{R}\mathbf{u}\right)dt = \int\begin{bmatrix}u_1\\ u_2\end{bmatrix}^\mathrm{T}\begin{bmatrix}R_{11} & R_{12}\\ R_{21} & R_{22}\end{bmatrix}\begin{bmatrix}u_1\\ u_2\end{bmatrix}dt \tag{8}$$

where $\mathbf{R}$ is a positive definite square matrix. In order to reach the optimum, its variation should satisfy

$$\delta J = 0 \Rightarrow \int\left(\delta\mathbf{u}^\mathrm{T}\left(\mathbf{R} + \mathbf{R}^\mathrm{T}\right)\mathbf{u}\right)dt = 0 \tag{9}$$

Considering Eq. (7) and fundamental lemma of calculus of variations [21], Eq. (9) yields the energy optimal ratio [19,20]

$$\beta^* \triangleq \frac{u_1}{u_2} = \frac{2R_{22}G_1^* - (R_{12}+R_{21})G_2^*}{2R_{11}G_2^* - (R_{12}+R_{21})G_1^*} \tag{10}$$

where superscript * represents the adjoint operator [22], which leads to a non-causal relationship between the control inputs that minimize J. As explained in [20], a causal approximation of the optimal relationship between the control inputs can be obtained by dropping the adjoint operator from Eq. (10), yielding

$$\beta \triangleq \frac{2R_{22}G_1 - (R_{12}+R_{21})G_2}{2R_{11}G_2 - (R_{12}+R_{21})G_1} \tag{11}$$

Here β is referred to as the approximate optimal control ratio, which is exactly optimal in the static sense but approximates energy optimality in the dynamic sense, due the elimination of the adjoint operator from Eq. (10) [20]; it is shown that β converges to optimality when $|\beta(j\omega)| \gg 1$, $|\beta(j\omega)| \ll 1$ and $\angle\beta(j\omega) \approx n\pi$ ($n \in \mathbb{Z}$) [20]. Under these conditions, it is

noteworthy that β specifies a (near) optimal control structure solely based on the specified energy index and system dynamics, without knowledge of the desired output and disturbance. Therefore, it can guide the (near) optimal distribution of the control efforts of redundant actuators without solving programming problems.

2.3. NEAR ENERGY OPTIMAL CONTROL ALLOCATOR

Control allocation is a methodology targeted at optimally distributing control efforts in over-actuated systems. A standard framework of control allocation is shown in Fig. 1. The overall controller is decomposed into two stages: the high level nominal controller, **C**, generates virtual control input $\mathbf{u}_0$, which is further distributed with control allocator **P** to generate actual control input **u**. As mentioned in Section 1, the first stage controller can be designed with various techniques; while the second stage, which is the major focus of control allocation, is traditionally achieved by solving programming problems.

The proposed method inherits the traditional two stage framework with three major differences. Firstly, the virtual control input, $\mathbf{u}_0$, is defined to be of n_u dimension instead of n_y as in [10]. This facilitates further decoupling of the two stages, as the system can be actuated with or without the allocator **P**. Note, however, that the traditional virtual control input of dimension n_y still fits within the proposed framework by assuming $n_u - n_y$ zero-input actuators. Secondly, the null space defined with steady state criteria in Eq. (4) is extended to all frequencies, enabling broadband, near energy optimal control allocation. Thirdly, the traditional programming problem in control allocator **P** is replaced by a simple LTI controller, thus reducing computational burden.

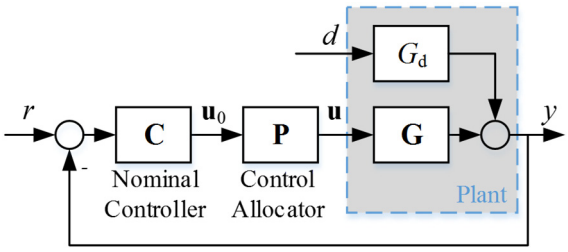

FIGURE 1: CONTROL ALLOCATION SCHEME

Control allocator **P** is designed to generate **u** from its optimization space $\Omega(\mathbf{u}_0)$, thus it does not change the plant output. According to Eq. (6), this can be explicitly expressed as

$$\mathbf{G}(\mathbf{u}_0 - \mathbf{u}) = 0 \Rightarrow \mathbf{u} = \mathbf{u}_0 + \begin{bmatrix} -G_2 \\ G_1 \end{bmatrix} \Delta u \tag{12}$$

where Δu is a free variable. For simplicity, an LTI allocator **P** is assumed. This requires Δu to be linearly related to either **u** or $\mathbf{u}_0$. It is mathematically equivalent to relate Δu to either **u** or $\mathbf{u}_0$. However, in this paper, we choose to relate Δu linearly to **u** instead of $\mathbf{u}_0$ because it streamlines the tuning process and enhances robustness of the resulting control allocator (as is further explained in the Appendix).

From energy efficiency point of view, the search of the best **u** in $\Omega(\mathbf{u}_0)$ is indirectly addressed by assuring maximum alignment of the elements of **u** with β, at frequencies where β is (near) optimal. It can be achieved in a linear system by minimizing the alignment deviation $u_1 - \beta u_2$ using a controller; i.e.,

$$\Delta u \triangleq H(u_1 - \beta u_2) = H\begin{bmatrix} 1 & -\beta \end{bmatrix}\mathbf{u} \tag{13}$$

where H is a scalar transfer function. In some sense, H follows a similar concept as the cross-coupling controller [23]; it manipulates the two control inputs towards a desirable alignment, by using the magnification of the alignment deviation $u_1 - \beta u_2$ in the feedback correction (shown in Fig. 2). The transfer function of **P** can therefore be derived as

$$\begin{bmatrix} u_1 \\ u_2 \end{bmatrix} = \underbrace{\frac{\begin{bmatrix} 1+\beta H G_1 & \beta H G_2 \\ H G_1 & 1+H G_2 \end{bmatrix}}{1+H G_2 + \beta H G_1}}_{=\mathbf{P}} \begin{bmatrix} u_{10} \\ u_{20} \end{bmatrix} \tag{14}$$

The proposed **P** can ensure that the output is not changed by the allocator, as can be verified by the fact that **GP** = **G**.

The allocator's influence, in terms of control alignment of **u** with β, can be evaluated as

$$u_1 - \beta u_2 = \frac{u_{10} - \beta u_{20}}{1 + H G_2 + \beta H G_1} \tag{15}$$

which shows the input-output relationship in terms of the alignments of $\mathbf{u}_0$ and **u** with β. Here

$$\theta(s) \triangleq 1 + H G_2 + \beta H G_1 \tag{16}$$

is crucial for the ability of **P** to shape a frequency dependent alignment of **u** with β for any given $\mathbf{u}_0$. The transfer function H can be shaped to give a large norm of θ at targeted frequency ranges where β is near optimal and energy efficiency is most desired (e.g., at the dominant frequencies of the disturbance input), as is discussed in Section 2.4.

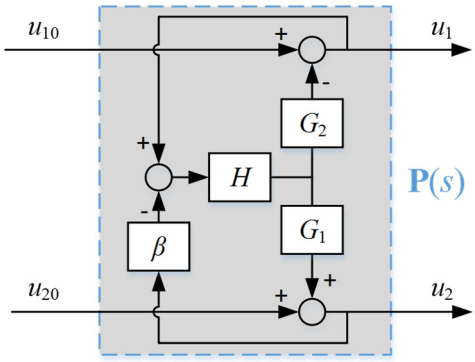

FIGURE 2: PROPOSED CONTROL ALLOCATOR

2.4. STABILITY AND DESIGN OF ALLOCATOR

Although the allocator does not change the input-output relationship of the system, it could affect the internal stability of the overall control system. The allocator **P** can be extracted

from the overall system dynamics, as in Fig. 3, to evaluate its effect on internal stability. According to [24], the system is internally stable if and only if all the input-output transfer functions in Fig. 3 are stable, i.e., the following four transfer functions

$$\begin{aligned}&\left(\mathbf{I}+\mathbf{PCG}\right)^{-1},\left(\mathbf{I}+\mathbf{PCG}\right)^{-1}\mathbf{P},\\&\left(\mathbf{I}+\mathbf{CGP}\right)^{-1},-\left(\mathbf{I}+\mathbf{CGP}\right)^{-1}\mathbf{CG}\end{aligned} \tag{17}$$

have no unstable poles. The stability of the inverted terms in Eq. (17) are guaranteed by the stability of the nominal controller **C** since

$$\det\left(\mathbf{I}+\mathbf{PCG}\right)=\det\left(\mathbf{I}+\mathbf{CGP}\right)=\det\left(\mathbf{I}+\mathbf{CG}\right) \tag{18}$$

The implication is that the allocator, **P**, is the only potential source of instability in Eq. (17). This fact indicates that the internal stability of the overall system can be guaranteed if and only if: (1) the original system without allocator **P** is stable; and (2) the allocator **P** is stable. Note that this property facilitates the decoupled design of allocator **P** and nominal controller **C**, which is very desirable in control allocation problems [10].

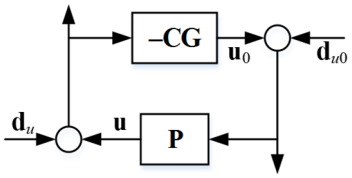

FIGURE 3: BLOCK DIAGRAM FOR INTERNAL STABILITY ANALYSIS

Notice that the absence of right hand plane zeros in $\theta(s)$ assures the stability of **P** (based on Eqs. (14) and (16)). Therefore, $\theta(s)$ deserves much focus as it is crucial to both system stability and allocation performance. The design of $\theta(s)$ is realized by the manipulation of H. Though a high-gain static H is likely to improve the allocation performance, it may reduce robustness and even cause instability. Here we assume that H is decomposed into a scalar gain, K_{AL}, and a dynamic term, H_0; i.e.,

$$H\left(s\right)=K_{\mathrm{AL}}H_0\left(s\right) \tag{19}$$

Based on Eq. (19), stable values of K_{AL} can be conveniently determined by standard root locus tools, by treating $H_0(G_2+\beta G_1)$ as an open loop plant and K_{AL} as a proportional feedback gain. Note $G_2+\beta G_1$ is not guaranteed to be minimum phase, even if β, G_1 and G_2 are each stable and minimum phase. H_0 should be designed to highlight particular frequencies of interest, while dealing with potential constraints on K_{AL} due to the presence of non-minimum phase effects [24]. The frequencies of interest can be acquired through some knowledge of the disturbance signal, or by observation of past control signals.

3. IMPLEMENTATION ON HYBRID FEED DRIVE

3.1. OVERVIEW OF HYBRID FEED DRIVE

Figure 4 illustrates the schematic of the dual-input over-actuated precision servo positioner used in this paper to demonstrate the proposed control allocation method. It is a hybrid feed drive (HFD) [25] consisting of a linear motor and a rotary motor which generates single degree of freedom linear motion through screw action via a reconfigurable Roh'lix® nut [26]. The Roh'lix® nut (which comes in two spring-loaded halves) acts as a clutch that can be opened to disengage it from the shaft, allowing the linear motor to act alone (during rapid motion). It can equally be closed to engage it with the shaft such that the linear motor and rotary motor can work in tandem to generate linear motion during cutting (e.g., milling).

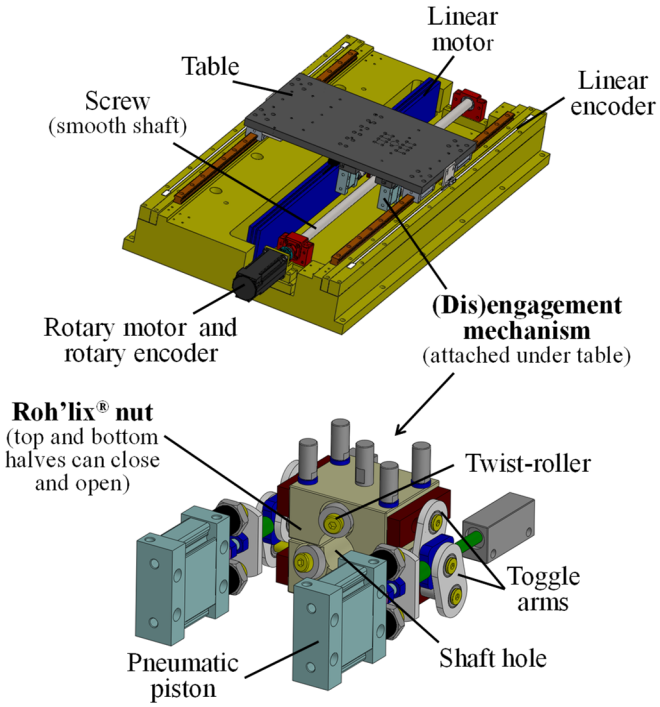

FIGURE 4: HYBRID FEED DRIVE WITH (DIS)ENGAGEMENT MECHANISM

Prior work by the authors [25] has demonstrated superior precision and significant improvements in energy efficiency (compared to a linear motor) as a result of the over-actuation of the HFD in its cutting mode. To achieve high precision and energy efficiency using the HFD, the right balance must be struck between actuation by the linear and rotary motors. The rotary motor is more energy efficient, while the linear motor provides higher system bandwidth. The objective of control allocation for the HFD is to improve energy efficiency without sacrificing positioning performance. This requires a broadband allocation scheme due to the difference in energy efficiency and frequency dependent maneuverability of the two actuators.

3.2. MODELING AND APPROXIMATE OPTIMAL CONTROL RATIO OF HYBRID FEED DRIVE

Similar to [19], the HFD is modeled as shown in Fig. 5 using a simple two-mass model given by

$$\begin{aligned} m_1\ddot{x}_1 + b_1\dot{x}_1 + c(\dot{x}_1 - \dot{x}_2) + k(x_1 - x_2) &= u_1 \\ m_2\ddot{x}_2 + b_2\dot{x}_2 + c(\dot{x}_2 - \dot{x}_1) + k(x_2 - x_1) &= u_2 + d \end{aligned} \tag{20}$$

where m_1 represents the equivalent mass of the rotor and shaft; m_2 is the mass of the table; x_1 and x_2 are the displacements of the two masses, with $y = x_2$ being the target for precision control; k, c, b_1, b_2 are the stiffness, damping and rigid body damping of the system; d is the disturbance force (dominated by cutting forces); u_1 and u_2 are the equivalent input forces to the two-mass system. The experimentally identified [19] parameters of the HFD's two-mass model are shown in Tab. 1. In transfer function format,

$$\begin{aligned} y = x_2 &= \begin{bmatrix} G_1 & G_2 \end{bmatrix} \begin{bmatrix} u_1 & u_2 \end{bmatrix}^{\mathrm{T}} + G_2 d \\ G_1 &= \frac{cs+k}{D_{\mathrm{ol}}};\ G_2 = \frac{m_1 s^2 + (c+b_1)s + k}{D_{\mathrm{ol}}} \\ D_{\mathrm{ol}} &= a_{\mathrm{ol},4}s^4 + a_{\mathrm{ol},3}s^3 + a_{\mathrm{ol},2}s^2 + a_{\mathrm{ol},1}s; \\ a_{\mathrm{ol},4} &= m_1 m_2;\ a_{\mathrm{ol},3} = b_1 m_2 + b_2 m_1 + c(m_1 + m_2) \\ a_{\mathrm{ol},2} &= c(b_1 + b_2) + k(m_1 + m_2) + b_1 b_2; \\ a_{\mathrm{ol},1} &= (b_1 + b_2)k \end{aligned} \tag{21}$$

where D_{ol} is the common denominator of the transfer function, while $a_{\mathrm{ol},i}$ (i=1,2,3,4) are its coefficients.

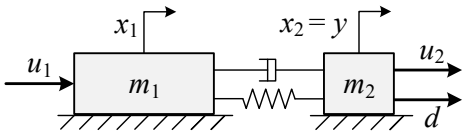

FIGURE 5: TWO-MASS MODEL OF HFD

TABLE 1: HFD'S TWO-MASS MODEL PARAMETERS

m_1 [kg]	616.2	b_1 [kg/s]	44.8	K_{m1}[N/$\sqrt{\mathrm{W}}$]	380.8
m_2 [kg]	46.3	b_2 [kg/s]	83.3	K_{m2}[N/$\sqrt{\mathrm{W}}$]	21
c [kg/s]	5777.2	k [N/μm]	3.1469	–	–

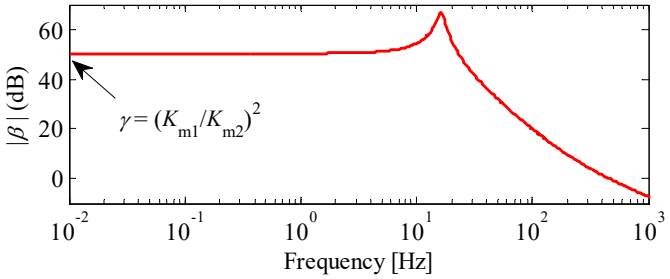

FIGURE 6: APPROXIMATE OPTIMAL CONTROL RATIO OF HFD

The energy cost functional for the HFD is modeled as the heat generated by its actuators during operation, i.e.

$$J = \int \left(\left(\frac{u_1}{K_{\mathrm{m1}}} \right)^2 + \left(\frac{u_2}{K_{\mathrm{m2}}} \right)^2 \right) dt \tag{22}$$

where K_{m1} and K_{m2} (shown in Tab. 1) are the motor constants of the rotary and linear motor, respectively. They represent the generic energy efficiency of the actuators, and ratio $\gamma = (K_{\mathrm{m1}}/K_{\mathrm{m2}})^2$ represents the energy optimal static control ratio. Equation (23) follows the general quadratic format in Eq. (8) with $R_{11} = (1/K_{\mathrm{m1}})^2$, $R_{22} = (1/K_{\mathrm{m2}})^2$, $R_{12} = R_{21} = 0$. Accordingly, the approximate optimal control ratio for the HFD, as defined in Eq. (11), can be calculated as

$$\beta = \left(\frac{K_{\mathrm{m1}}}{K_{\mathrm{m2}}} \right)^2 \frac{G_1}{G_2} = \gamma \frac{cs + k}{m_1 s^2 + (c + b_1)s + k} \tag{23}$$

Note that this ratio combines the knowledge of the actuators' frequency dependent maneuverability with their energy cost. As depicted for the HFD in the Bode plot of Fig. 6, at low frequencies ($s \to 0$), $\beta \to \gamma$, as is employed in traditional static allocation methods. However, at higher frequencies, β deviates quite significantly from γ, which exposes the inadequacy of the traditional static allocation methods. For instance, at very high frequencies (i.e., $s \to \infty$) $\beta \to 0$, meaning that all actuation effort should be allocated to the linear motor. This is desirable since the rotary motor cannot effectively control the table at very high frequencies because of the mechanical decoupling effect of the two-mass system [27]. It has been shown in [20] that, for the HFD, the worst case approximation in β relative to the exact optimal ratio is small at all frequencies; therefore it can be considered to be near optimal regardless of the frequencies of interest.

3.3. NEAR ENERGY OPTIMAL CONTROL ALLOCATOR DESIGN FOR HFD AND SIMULATION RESULTS

Section 2.4 has demonstrated that the controller and allocator can be designed separately. It can be verified that $G_2 + \beta G_1$ has a pair of complex conjugate non-minimum phase zeros. Therefore, following the design guidelines presented in Section 2.4, $H_0(s)$, the dynamic portion of H, is designed to magnify frequencies where β is near optimal and minimal alignment deviation is desired. Accordingly, $H_0(s)$ is defined as

$$H_0(s) = W_d(s) \frac{D_{\mathrm{ol}}(s)}{D_{\mathrm{d}}(s)} \tag{24}$$

where $W_d(s)$ is a transfer function that helps amplify the frequencies of interest. The term $D_{\mathrm{ol}}(s)/D_{\mathrm{d}}(s)$ is introduced such that the common denominator of the original system, D_{ol}, containing undesirable structural modes, is replaced by a user defined denominator, D_{d}. We recommend designing D_{d} as a low pass filter whose cutoff frequency determines the desired bandwidth for the control allocator, **P**. For the purpose of our simulations, the bandwidth of **P** is selected as 100 rad/s, at

which frequency a third order Butterworth low pass filter, D_d, is defined.

In order to define suitable $W_d(s)$, two nominal disturbance profiles, each with added white noise of $\sigma^2 = 50$ N^2, are considered:

(a) Constant disturbance: $d = 100$ N

(b) Sinusoidal disturbance at 10Hz: $d = 100\sin(20\pi t)$ N

Accordingly, for Case (a), $W_d(s)$ is defined as a simple integrator, i.e., $W_d(s) = W_{d,1}(s) = 1/s$. For Case (b),

$$W_d(s) \triangleq W_{d,2}(s) = \frac{1}{s}\frac{\omega_0^2}{s^2 + 2\zeta\omega_0 s + \omega_0^2} \tag{25}$$

where $\omega_0 = 20\pi$ rad/s (i.e. 10Hz) and $\zeta = 0.1$ are used. In other words, for both cases, the internal model principle [28] is employed in $W_d(s)$ for magnifying the targeted frequency ranges. Note that $W_{d,2}$ also contains an integrator. This is recommended for practical situations where static control effort allocation is unavoidable due to static disturbances like friction.

Note that the static optimal control ratio of the HFD, i.e., $\gamma = (K_{m1}/K_{m2})^2 \approx 329$, indicating the high efficiency of rotary motor actuation relative to the linear motor. However, this large value of γ makes it a bit difficult to illustrate the performance of the proposed allocator in plots showing u_1 and u_2. Therefore, $K_{m1} = 2$ N/$\sqrt{\text{W}}$ and $K_{m2} = 1$ N/$\sqrt{\text{W}}$ (i.e., $\gamma = 4$) are used for better illustrating the performance of the proposed allocator in simulations.

The root locus designs for $W_{d,1}$ and $W_{d,2}$ are illustrated in Fig. 7. The solid square markers in Fig. 7 represent the poles of allocator **P**, generated using a common $K_{AL} = 3$. Note that the shape of the root locus plot of Fig. 7(b) is significantly different from that of Fig. 7(a) due to the placement of poles near the imaginary axis by $W_{d,2}$. The real part of the slowest pole is changed from –9.4 s^{-1} to –4 s^{-1} for cases with $W_{d,1}$ and $W_{d,2}$, which reflects a drop of the settling time in reaching steady state. In other words, perfect alignment at finite frequency ω_0 is achieved at the cost of robustness and settling time. Notice that there are zeros in the right hand plane of both root locus plots which indicate, as mentioned earlier, that $G_2+\beta G_1$ is non-minimum phase.

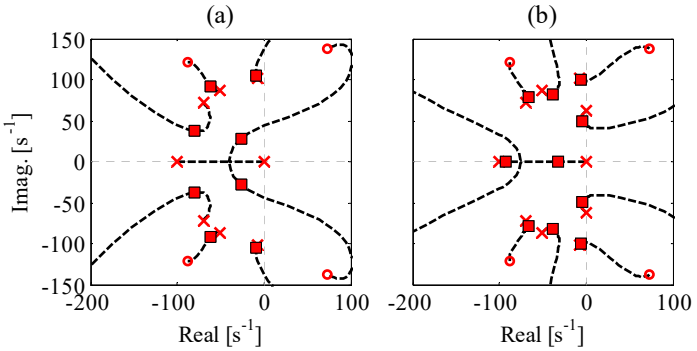

FIGURE 7: ROOT LOCUS DESIGN WITH (a) $W_{d,1}(s)$ AND (b) $W_{d,2}(s)$

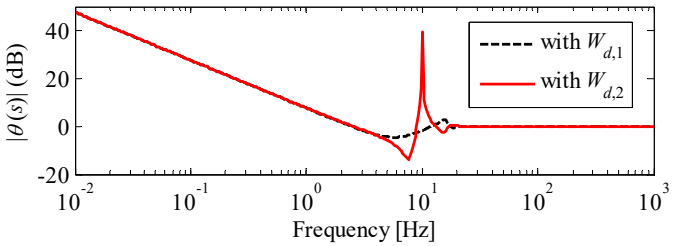

FIGURE 8: MAGNITUDE OF $\theta(s)$

The magnitude of the critical $\theta(s)$ in Eq. (16) is plotted in Fig. 8. It is shown that magnification at certain frequency ranges of H can effectively manipulate the shape of $\theta(s)$. The approximate control ratio, β, along with the actual control ratio (u_1/u_2) for the two designs, are plotted in Fig. 9. Notice that the modification of motor constants causes a magnitude shift in β; its magnitude starts from 4 (12dB) at low frequencies and follows same shape of the original ratio (shown in Fig. 6). However, using the criterion defined in [20], it can be verified that this modified ratio is still near optimal at all frequencies. Observe from Fig. 9 that, thanks to the integrator, the two designs converge to β at low frequencies. Moreover, due to the additional resonance term, $W_{d,2}$ achieves perfect alignment with β at 10Hz; note that at 10 Hz the phase of Case (b) has a severe drop such that it coincides with β (with 360° phase difference).

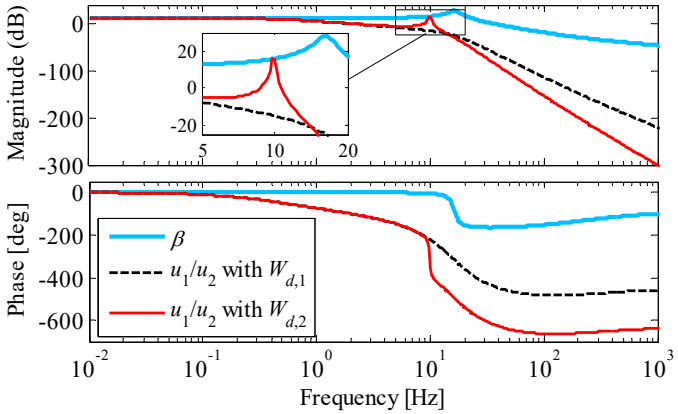

FIGURE 9: APPROXIMATE ENERGY OPTIMAL CONTROL RATIO AND ACTUAL CONTROL RATIO OF HFD (USING MODIFIED MOTOR CONSTANTS)

The proposed allocator's effects on different disturbance profiles are validated in time domain simulation. To simplify the analysis, the nominal controller, **C**, is designed as a PID controller using only u_2 for actuation. Here u_2 is chosen since the allocator does not redistribute the high-frequency actuation (i.e., it does not affect $\mathbf{u}_0$ beyond 100 rad/s bandwidth). Therefore, the nominal controller **C** must be designed to align closely with the high-bandwidth actuator (i.e., u_2). Thus,

$$\mathbf{C}(s) = \begin{bmatrix} 0 & K_p + \frac{K_i}{s} + \frac{K_d s}{T_f s + 1} \end{bmatrix}^T \tag{26}$$

where K_p=3.15×10^6 N·m^{-1}, K_i=1.72×10^6 N·m^{-1}·s^{-1}, K_d =5.62×10^4 N·m^{-1}·s, T_f =1.39×10^{-4} s are calculated using Matlab's® PID tuning tool targeted at a crossover frequency of 10 rad/s. This configuration also demonstrates how the dimension of $\mathbf{u}_0$ can be expanded by defining zero-input actuation (as explained in Section 2.1). The performance of the proposed allocator is compared with the allocator proposed in [15], where energy performance matrix $\overline{\boldsymbol{W}}$=diag($K_{m1}^{-2}$,$K_{m2}^{-2}$) and allocator speed parameter K=10 are used.

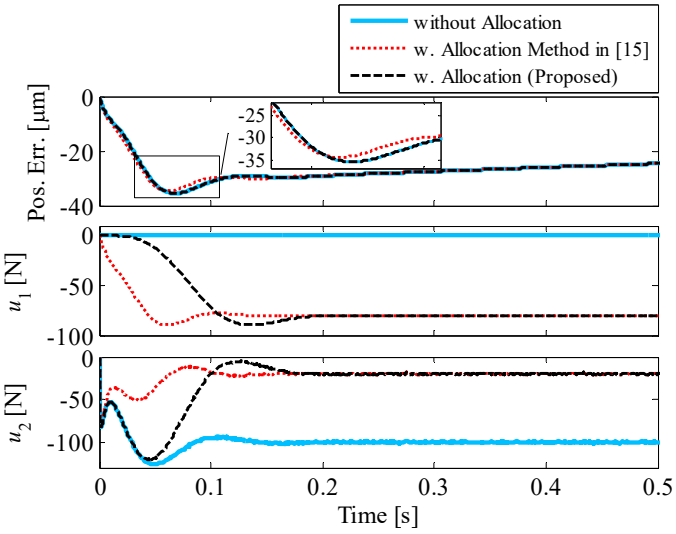

FIGURE 10: CONTROL ALLOCATION RESULTS WITH PID CONTROLLER FOR CONSTANT DISTURBANCE d = 100 N WITH ADDED WHITE NOISE OF σ^2 = 50 N^2

The regulation of the constant disturbance (i.e. Case (a)) from the two actuators is shown in Fig. 10. It is shown that, under static disturbance, both allocation methods can distribute the control effort in an energy efficient manner. Also, the high frequency white noise introduced into the system is totally regulated by u_2. Notice that, compared to the allocation method proposed in [15], the proposed method does not change the system output; i.e., the output of the proposed method is exactly the same as that from the nominal controller. This demonstrates the difference between the traditional static allocation and broadband allocation proposed in this paper. This difference is further illustrated in Case (b) with sinusoidal disturbance, as shown in Fig. 11. In this case, the steady state responses of the system are drastically different, in that the proposed method uses significant less u_2 in resisting the disturbance at ω_0.

The transient power consumption (computed by considering only the simulated time frame, shown in Figs. 10 and 11) and the steady state power consumption for the two disturbance profiles are summarized in Tab. 2, where P_1, P_2, and P_{total} are defined as the average power consumption of u_1, u_2 and their combination. For Case (a), both the allocator in [15] and the proposed allocator can significantly reduce the energy consumption (up to 80%) compared to using u_2 alone. The performance of the two allocators converges to the optimum at steady state; however, the proposed method consumes more power during transients since the method proposed in [15] is tuned to have a higher convergence speed. For Case (b) with disturbance at ω_0, the energy optimization of the method in [15] is limited by its static model, and therefore only provides 23% and 19% power consumption advantage compared to the case without allocation in transient and steady state operation, respectively. The proposed method is shown to be capable of further increasing energy efficiency due to its complete dynamic model and near optimal β. Compared with the allocator in [15], the proposed allocator consumes 66% and 89% less power, during its transient and steady state operation, respectively.

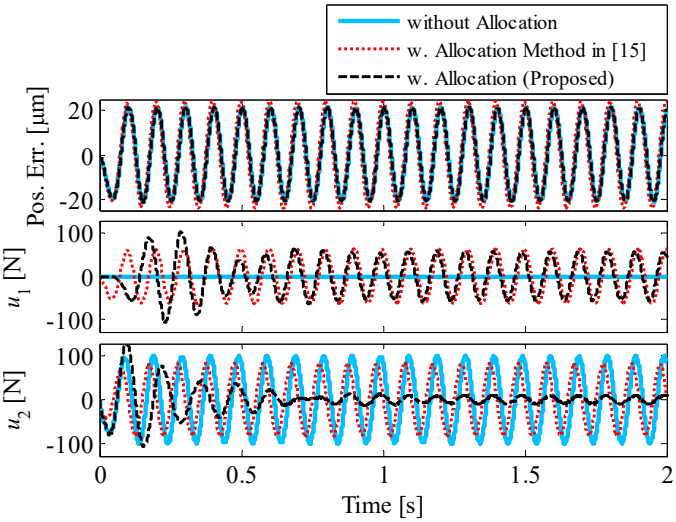

FIGURE 11: CONTROL ALLOCATION RESULTS WITH PID CONTROLLER FOR SINUSOIDAL DISTURBANCE d = 100sin(20πt) N WITH ADDED WHITE NOISE OF σ^2 = 50 N^2

TABLE 2: POWER CONSUMPTION COMPARISON

		With Transients [W]			Steady State [W]		
		P_1	P_2	P_{total}	P_1	P_2	P_{total}
(a)	Without allocation	0	10058	10058	0	10000	10000
	Allocator in [15]	1534	586	2119	1600	400	2000
	Proposed allocator	1367	1733	3100	1600	400	2000
(b)	Without allocation	0	4954	4954	0	5000	5000
	Allocator in [15]	509	3314	3823	517	3511	4029
	Proposed allocator	481	826	1307	407	56	463

3.4. EXPERIMENTAL RESULTS

The proposed allocation method is evaluated in experiments conducted on an in-house built prototype of the HFD of Fig. 4 (see [25] for details), controlled at 10 kHz sampling frequency using dSPACE DS1103 control board. In

the experiments, the output, $y = x_2$, is commanded to track the snap limited trajectory (see [29]) whose parameters are given in Tab. 3. Between 1 and 4 s, during the constant velocity portion of the motion, disturbance force $d = -(100\sin(20\pi t) + 100)$ N is applied to the HFD's table through the linear motor. Note that the applied biased sinusoidal disturbance profile, which combines cases (a) and (b) studied in simulations above, mimics the constant and the dominant harmonic of cutting forces acting against the motion of the table during milling operations [19].

TABLE 3: TRAJECTORY PARAMETERS

X_{lim} [mm]	V_{lim} [mm·s^{-1}]	A_{lim} [mm·s^{-2}]	J_{lim} [mm·s^{-3}]	S_{lim} [mm·s^{-4}]
50	10	100	6.25×10^3	1.25×10^6

The simple PID controller employed in Section 3.3 is not suitable as the nominal controller for tracking experiments on the HFD because the Roh'lix® nut (see Fig. 4) is a friction drive; using solely the linear motor for actuation will drag the nut along the smooth shaft, causing extensive wear and change of transmission ratio. Therefore, a P-PI/PD controller optimized for disturbance rejection [30] is used as the nominal controller $\mathbf{C}(s)$; the P-PI controller is applied to the rotary motor while the PD controller is used for the linear motor.

The design of allocator follows same methodology as in Section 3.3, based on $W_{d,2}$ defined in Eq. (25), since the disturbance profile contains both static and harmonic components. The root locus design yields $K_{AL} = 0.04$ based on the authentic motor constants of the HFD defined in Tab. 1.

The experimental tracking errors and control signals for the three allocation cases considered in simulations are shown in Fig. 12, with relevant statistics summarized in Tab. 4. One observes that the tracking performances of the three cases are similar; their RMS and peak tracking errors are all within 9% of each other. Notice, however, that unlike in simulations, the proposed allocation's replication of the nominal controller's tracking performance is not perfect. This slight discrepancy could be attributed to modeling errors and nonlinearities (like micro-slip between the Roh'lix® nut and shaft [29]).

The frequency spectra of the control signals are plotted in Fig. 13, to add more clarity to their time domain signals plotted in Fig. 12. It can be seen that the differences in the power consumption of the three cases are primarily due to the linear motor's control effort (u_2). When system is controlled solely by the nominal controller (i.e. without allocator), about 12% of static cutting force is counteracted using the linear motor, although the P-PI/PD controller employed was designed to be energy efficient [30]. When either allocator is introduced, this percentage drops to almost zero because of the large static energy efficient control ratio γ ($\approx$ 329), as discussed in Section 3.3. The difference in power consumption between the allocation method in [15] and the proposed allocator occurs at 10 Hz where significant cutting energy is concentrated. The allocator in [15] barely changes the control effort at 10 Hz; However, in keeping with β whose magnitude is plotted Fig. 6, the proposed method uses much less linear motor effort at the expense of a modest increase in rotary motor effort. As a result, as indicated in Tab. 4, the proposed method achieves almost same tracking performance with 89% less energy consumption in this specific case study.

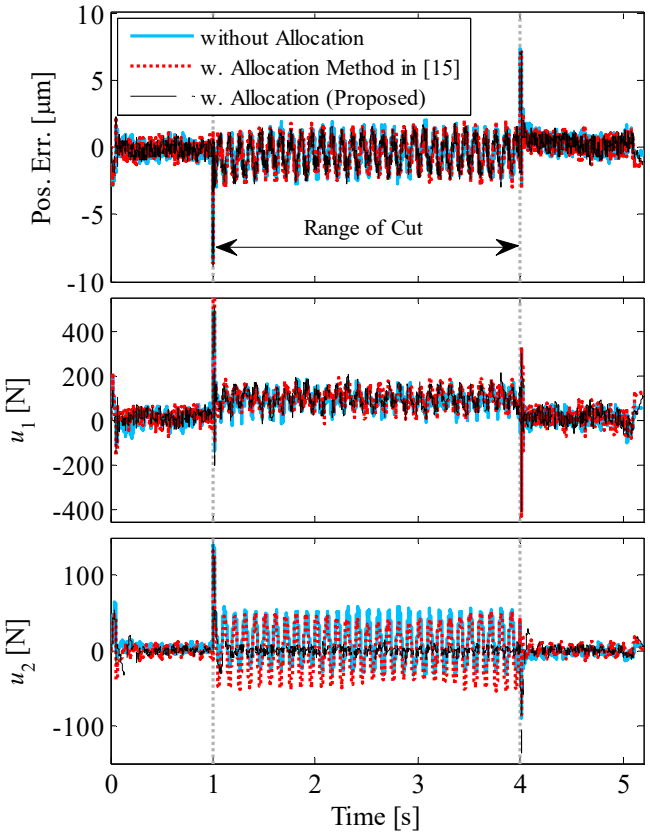

FIGURE 12: TRACKING ERRORS AND CONTROL EFFORT COMPARISON FOR DIFFERENT ALLOCATION SCHEMES (EXPERIMENTS)

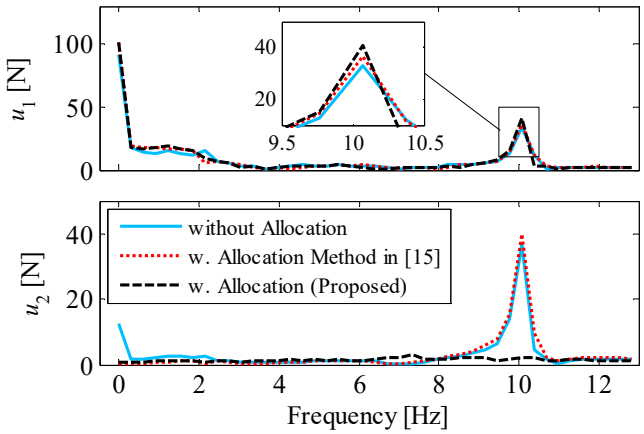

FIGURE 13: SINGLE-SIDED SPECTRUM OF THE CONTROL INPUTS u_1 AND u_2 OVER THE RANGE OF CUT

TABLE 4: POSITIONING PERFORMANCE AND AVERAGE POWER CONSUMPTION COMPARISON OVER THE RANGE OF CUT

	Pos. Err. [μm]		**Power** [mW]		
	Max.	RMS	P_1	P_2	P_{total}
Without allocation	8.38	0.93	67.8	2168.6	2236.4
Allocator in [15]	8.66	1.01	81.6	2248.8	2330.4
Proposed allocator	8.98	0.94	82.9	165.4	248.3

4. CONCLUSION AND FUTURE WORK

An elegant method for near energy optimal control allocation for dual-input, over-actuated systems is proposed. An energy optimal control ratio is defined, representing the relationship that must be maintained between the two control inputs to ensure energy optimality without sacrificing positioning performance. Due to the non-causality of the optimal control ratio, an approximate optimal control ratio, which is near energy optimal under specific conditions, is deduced. Energy efficient control allocation is achieved by using an LTI controller to align any given control inputs with the approximate optimal control ratio at frequencies of interest where the approximate ratio is (near) optimal.

The key benefits of the proposed method relative to existing methods lie in its ability to achieve near optimal control allocation: (i) with low computational burden; (ii) without sacrificing positioning performance; and (iii) over a broad range of frequencies. The proposed method is compared with an existing allocation method in simulations and experiments conducted on an over-actuated hybrid feed drive. Significant improvements in energy efficiency without sacrificing positioning accuracy are demonstrated. Future work will generalize the proposed method to multi-input multi-output over-actuated systems. Issues of robustness and actuator constraints will also be addressed.

ACKNOWLEDGEMENTS

This work is funded by the National Science Foundation's CAREER Award #1350202: Dynamically Adaptive Feed Drives for Smart and Sustainable Manufacturing.

REFERENCES

[1] Halevi, Y., Carpanzano, E., and Montalbano, G., 2014, "Minimum Energy Control of Redundant Linear Manipulators," J. Dyn. Syst. Meas. Control, 136(5), p. 051016.

[2] Zheng, J., Su, W., and Fu, M., 2010, "Dual-Stage Actuator Control Design Using a Doubly Coprime Factorization Approach," IEEE/ASME Trans. Mechatronics, 15(3), pp. 339–348.

[3] Ronde, M. J. C., Schneiders, M. G. E., Kikken, E. J. G. J., van de Molengraft, M. J. G., and Steinbuch, M., 2014, "Model-based Spatial Feedforward for Over-actuated Motion Systems," Mechatronics, 24(4), pp. 307–317.

[4] Servidia, P. A., and Pena, R. S., 2005, "Spacecraft Thruster Control Allocation Problems," IEEE Trans. Automat. Contr., 50(2), pp. 245–249.

[5] Chen, Y., and Wang, J., 2014, "Adaptive Energy-Efficient Control Allocation for Planar Motion Control of Over-Actuated Electric Ground Vehicles," IEEE Trans. Control Syst. Technol., 22(4), pp. 1362–1373.

[6] Tagesson, K., Sundstrom, P., Laine, L., and Dela, N., 2009, "Real-time Performance of Control Allocation for Actuator Coordination in Heavy Vehicles," Intell. Veh. Symp. 2009 IEEE, pp. 685–690.

[7] Brinkerhoff, R., and Devasia, S., 2000, "Output Tracking for Actuator Deficient/Redundant Systems: Multiple Piezoactuator Example," J. Guid. Control. Dyn., 23(2), pp. 370–373.

[8] Cheng, H., Yiu, Y. K., and Li, Z., 2003, "Dynamics and Control of Redundantly Actuated Parallel Manipulators," IEEE/ASME Trans. Mechatronics, 8(4), pp. 483–491.

[9] Oppenheimer, M. W., Doman, D. B., and Bolender, M. a., 2006, "Control Allocation for Over-actuated Systems," 14th Mediterr. Conf. Control Autom. MED'06, (2).

[10] Johansen, T. A., and Fossen, T. I., 2013, "Control Allocation - A Survey," Automatica, 49(5), pp. 1087–1103.

[11] Härkegård, O., 2003, "Backstepping and Control Allocation with Applications to Flight Control," Linköping University.

[12] Bodson, M., 2002, "Evaluation of Optimization Methods for Control Allocation," J. Guid. Control. Dyn., 25(4), pp. 703–711.

[13] Härkegård, O., 2004, "Dynamic Control Allocation Using Constrained Quadratic Programming," J. Guid. Control. Dyn., 27(6), pp. 1028–1034.

[14] Burken, J. J., Lu, P., Wu, Z., and Bahm, C., 2001, "Two Reconfigurable Flight-Control Design Methods: Robust Servomechanism and Control Allocation," J. Guid. Control. Dyn., 24(3), pp. 482–493.

[15] Zaccarian, L., 2009, "Dynamic Allocation for Input Redundant Control Systems," Automatica, 45(6), pp. 1431–1438.

[16] Härkegård, O., and Glad, S. T., 2005, "Resolving Actuator Redundancy - Optimal Control vs. Control Allocation," Automatica, 41(1), pp. 137–144.

[17] Petersen, J. A. M., and Bodson, M., 2006, "Constrained Quadratic Programming Techniques for Control Allocation," IEEE Trans. Control Syst. Technol., 14(1), pp. 91–98.

[18] Zhou, J., Canova, M., and Serrani, A., 2016, "Predictive Inverse Model Allocation for Constrained Over-actuated Linear Systems," Automatica, 67, pp. 267–276.

[19] Duan, M., and Okwudire, C., 2015, "Energy-efficient Controller Design for a Redundantly-actuated Hybrid Feed Drive with Application to Machining," IEEE/ASME Trans. Mechatronics.

[20] Duan, M., and Okwudire, C. E., "Correction to 'Energy-efficient Controller Design for a Redundantly-actuated Hybrid Feed Drive with Application to Machining,'" Submitt. to IEEE/ASME Trans. Mechatronics.

[21] Komzsik, L., 2014, Applied Calculus of Variations for Engineers, CRC Press.
[22] Beard, R. W., 2002, "Linear Operator Equations with Applications in Control and Signal Processing," IEEE Control Syst. Mag., 22(2), pp. 69–79.
[23] Koren, Y., and Lo, C.-C., 1991, "Variable-Gain Cross-Coupling Controller for Contouring," CIRP Ann. - Manuf. Technol., 40(1), pp. 371–374.
[24] Skogestad, S., and Postlethwaite, I., 2007, Multivariable Feedback Control: Analysis and Design, Wiley New York.
[25] Okwudire, C., and Rodgers, J., 2013, "Design and Control of a Novel Hybrid Feed Drive for High Performance and Energy Efficient Machining," CIRP Ann. - Manuf. Technol., 62(1), pp. 391–394.
[26] "Roh'Lix® Linear Actuators" [Online]. Available: http://www.zero-max.com/linear-motion-control-c-24-l-en.html. [Accessed: 01-Dec-2015].
[27] Schmidt, R. M., Schitter, G., and Rankers, A., 2014, The Design of High Performance Mechatronics: High-Tech Functionality by Multidisciplinary System Integration, IOS Press.
[28] Francis, B. A., and Wonham, W. M., 1976, "The Internal Model Principle of Control Theory," Automatica, 12(5), pp. 457–465.
[29] Duan, M., and Okwudire, C. E., 2016, "Modeling and Observer-Based Compensation of Slip in a Friction Drive for Servo Positioning," 2016 International Symposium on Flexible Automation, Cleveland, OH.
[30] Duan, M., and Okwudire, C., 2015, "Energy Efficiency and Performance Optimized Control of a Hybrid Feed Drive," ASME 2015 International Manufacturing Science and Engineering Conference, Charlotte, NC.

APPENDIX: LINEAR CONTROL ALLOCATOR EQUIVALENCE

The mathematical equivalence of using $\mathbf{u}_0$ and $\mathbf{u}$ in Eq. (13) is shown in following derivation. Equation (14) can be written as

$$\begin{bmatrix} u_1 \\ u_2 \end{bmatrix} = \begin{bmatrix} u_{10} \\ u_{20} \end{bmatrix} + \frac{\begin{bmatrix} -HG_2 & \beta HG_2 \\ HG_1 & -\beta HG_1 \end{bmatrix}}{1 + HG_2 + \beta HG_1} \begin{bmatrix} u_{10} \\ u_{20} \end{bmatrix} \tag{27}$$

which can be organized as

$$\begin{aligned} \mathbf{u} &= \mathbf{u}_0 + \begin{bmatrix} -G_2 \\ G_1 \end{bmatrix} \bar{H} \begin{bmatrix} 1 & -\beta \end{bmatrix} \mathbf{u}_0 \\ \bar{H} &\triangleq \frac{H}{1 + HG_2 + \beta HG_1} \end{aligned} \tag{28}$$

Note that this yields same configuration as Eqs. (12) and (13) with different H (defined by $\bar{H}$ in this case). Note that in this case the alignment effect is expressed as

$$u_1 - \beta u_2 = \left(1 - \bar{H}G_2 - \beta \bar{H}G_1\right)\left(u_{10} - \beta u_{20}\right) \tag{29}$$

which, in order to minimize $u_1 - \beta u_2$, requires

$$1 - \bar{H}G_2 - \beta \bar{H}G_1 \to 0 \Rightarrow \bar{H} \to \frac{1}{G_2 + \beta G_1} \tag{30}$$

Notice that the input-output relationship in terms of the alignments of $\mathbf{u}_0$ and $\mathbf{u}$ with β in Eq. (29) has a feedforward control structure, compared to that in Eq. (15) which has a feedback control structure. Therefore, the relationship in Eq. (15) facilitates the design/tuning of a robust allocator H, compared to $\bar{H}$ given in Eq. (30) which leaves no room for tuning and, to be effective, requires an accurate plant model. For this reason, in Section 2.3, we have chosen to express Δu as a linear function of $\mathbf{u}$ instead of $\mathbf{u}_0$.